Quantifying memory: Detection of focal conic domain rearrangement across a phase transition Supplemental materials

Sean Hare, Alexander de la Vega and Francesca Serra

1 Binomial and Weighted Error Calculation

For calculations of conditional probability we assume binomial uncertainties. The conditional probability and associated uncertainty are calculated separately for each temperature ramp and assigned a weight to be used in successive calculations. All values plotted in Figures 5–6 in the main text and in the Supplemental Materials were calculated using a weighted mean of these measurements. The weight is the product of two component weights, i.e. $w = w_{ext} \times w_{err}$. The first component weight w_{ext} is the external weight—equal to the quantity of microchannels tested for that particular measurement. The second component weight w_{err} is the standard error (inverse-variance) for that measurement.

Figures 5 and 6 are both calculated in this manner, and the only difference between the plots is that Figure 6 had data grouped according to their geometry before applying the weighted mean. The restricted data sets plotted in Figure 6, each having a smaller effective number of measurements, have much larger associated error.

For calculating the standard error of the weighted mean of differently-weighted values, we estimate the effective number of measurements[1,2] as n_{eff},

$$n_{eff} = \frac{\left(\sum_i^n w_i\right)^2}{\sum_i^n w_i^2} \tag{S1}$$

where w_i are the combined weights $w_{ext} \times w_{err}$.

For many of the values $N_{events} = N_{total}$ (Figure S1(a); black pentagons). This is problematic because the associated binomial error is zero (Figure S1(b); black pentagons). To account for this, we apply a correction specifically for these values. We first look at nearby values along the curve of constant N_{total}. In Figure S1(a) these correspond to horizontal lines and in Figure S1(b) these are downward parabolas. The error of the nearest point along this parabola ($N_{events} = N_{total} - 1$) is averaged with zero (corresponding to black pentagons). The final 'corrected' values are represented by red stars in Figure S1(b), with dashed red lines indicating the value they are correcting.

One additional note is that this correction was also applied to $N_{events} = 0$ for all values of N_{total}. On Figure S1(b) this is represented by multiple identical overlapping values at (0,0), with the corresponding corrections not shown.

[1] James W. Kirchner. *Data Analysis Toolkit 12: Weighted averages and their uncertainties*. 2006. URL: http://seismo.berkeley.edu/~kirchner/Toolkits/Toolkit_12.pdf.

[2] Philip R. Bevington. *Data Reduction and Error Analysis for the Physical Sciences*. McGraw-Hill Companies, 1969.

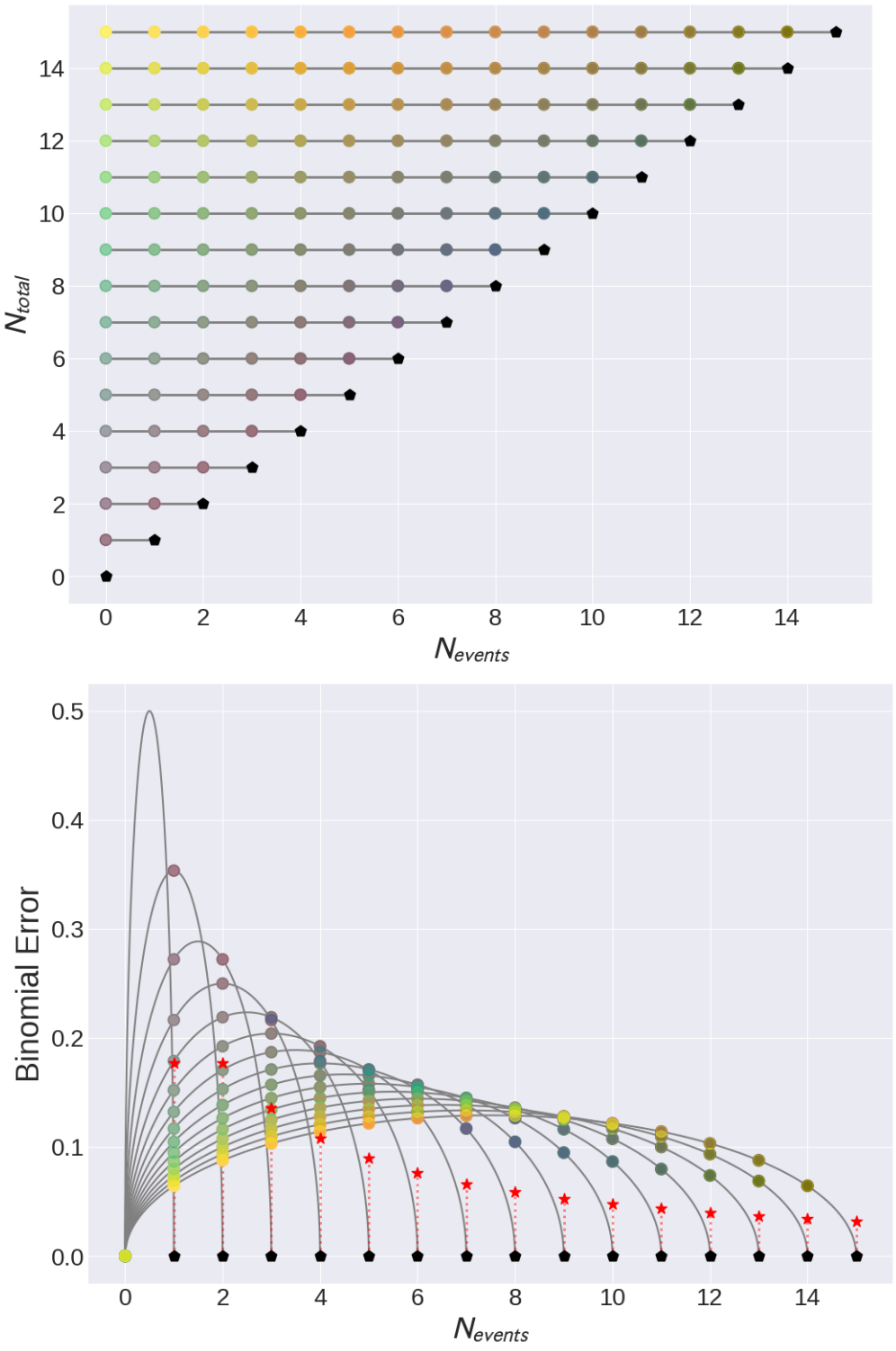

Figure S1: Simulated scatter plots of values (for $N_{total} \leq 15$) used to perform a non-zero correction to the binomial error. Each point in (a) corresponds to a point in figure (b) with matching color. Lines correspond to fixed values of N_{total}. Black pentagons indicate unity ($N_{event} = N_{total}$) and are uncorrected values using the standard binomial error definition. Each pentagon corresponds to a red star in figure(b)—a corrected value calculated by averaging the three nearest values along the same N_{total} line.

2 Supplemental Figures

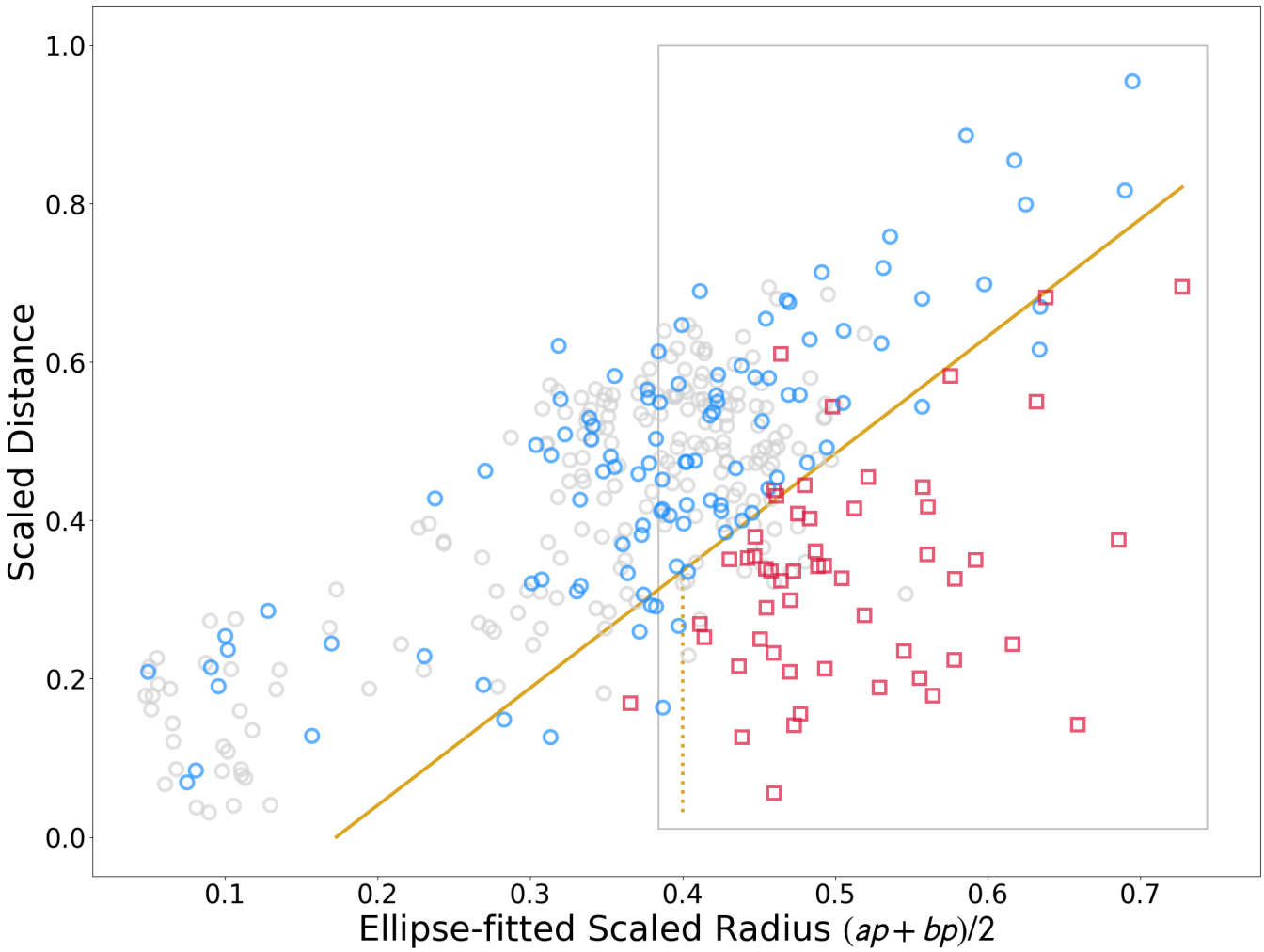

Figure S2: Full distribution of FCD size and distance from the center of their closest pockets for data shown in Figure 4 of the main text, which only shows a portion of the full distribution corresponding to the grey rectangular box. Here we show also the FCDs that are below the cutoff size, represented by the vertical dashed line (corresponding to Scaled Radius = 0.32). The plot shows that there are indeed many FCDs that are too small to be considered in our subsequent analysis. Another good reason to ignore these small FCDs is that some of them are artifacts from the segmentation method. In our program for detection of large FCDs, these are all filtered out.

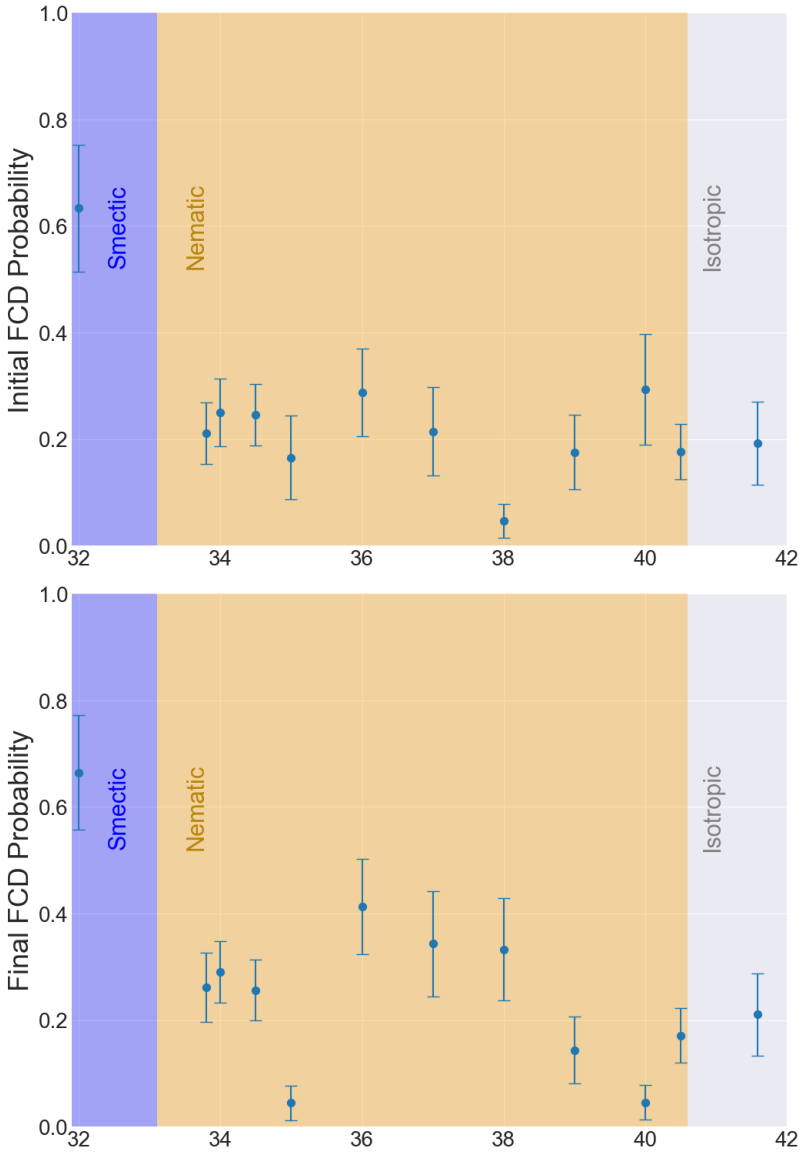

Figure S3: Initial FCD probability, $P(FCD_{i-1})$ (top plot) and final FCD probability $P(FCD_i)$ (bottom plot) vs. the maximum heating temperature T_H. $P(FCD_{i-1})$ and $P(FCD_i)$ represent the formation rate of large FCDs before and after heated to nematic, respectively. $P(FCD_i)$ is the baseline value before anything has occurred, which we expect to be perfectly flat, and we also expect $P(FCD_f)$ to be flat as well, to confirm that there were no major trends across temperatures. An important feature is that there is no significant consistent increase/decrease between $P(FCD_i)$ and $P(FCD_f)$. In other words, the overall shape of the data remains mostly unchanged after heating. While there may be some evolution in the size/distance distribution (not represented by this plot), a general increase/decrease in the total formation of large FCDs is not a significant enough effect to explain the geometric memory we observe.

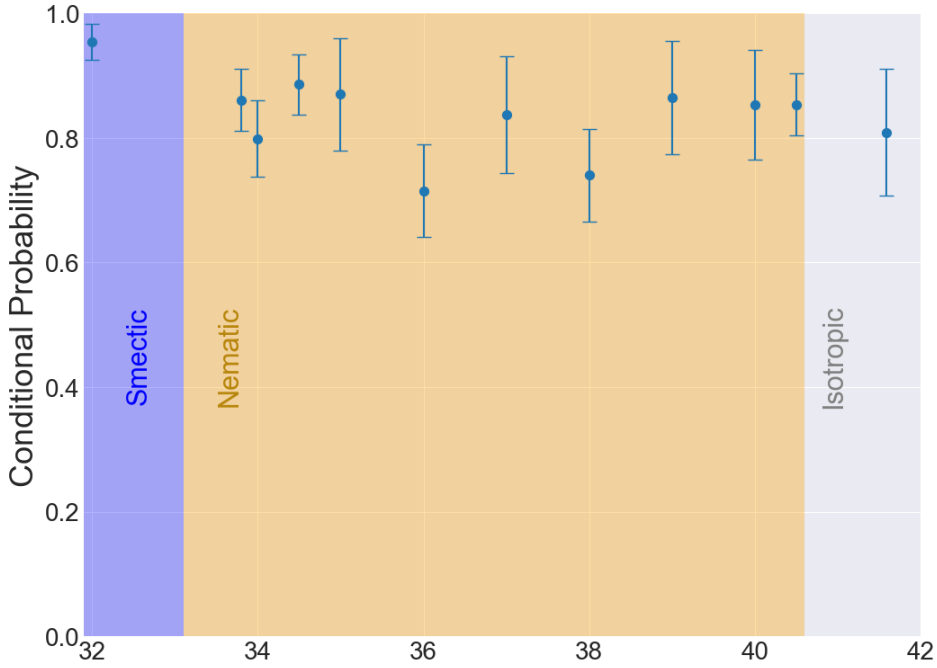

Figure S4: Conditional Probability $P(\overline{FCD}_i|\overline{FCD}_{i-1})$ vs. the maximum heating temperature T_H. The graph shows that this quantity is not influenced by the heating temperature, as expected. If initially no FCD is present in a pocket, the probability that a FCD will not form there at a later stage is temperature-independent.

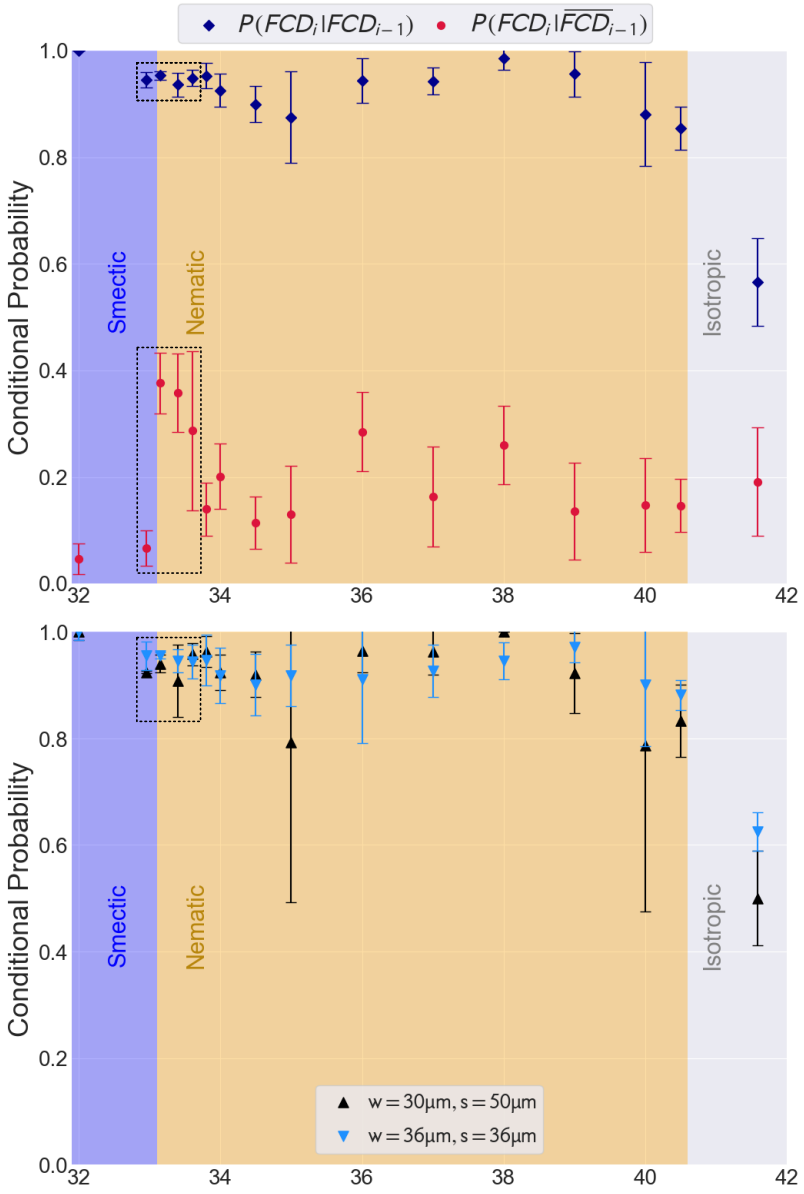

Figure S5: Conditional Probabilities: $P(FCD_i|FCD_{i-1})$ (top figure, dark blue diamonds) and $P(FCD_i|\overline{FCD}_{i-1})$ (top figure, red circles) vs. the maximum heating temperature T_H. Conditional Probability $P(FCD_i|FCD_{i-1})$ (bottom figure) vs. T_H, with data grouped according to their geometry (w,s). The plotted data in the top and bottom figures are like Figures 5 and 6 in the paper, respectively, but they include additional data (indicated in boxes) across the smectic-nematic phase transition (32.9-33.6C range). The reason for excluding these data from the main paper is that the images were taken at a later time (about 3 months later), after the sample had partially degraded. The overall rate of formation of FCDs is larger for these additional data points (so $P(FCD_i)$ is abnormally high). Despite this, $P(FCD_i|FCD_{i-1})$ is consistently reduced compared to the data point at 32C, even when the sample is barely heated such that T_H does not exceed the Sm-Nm transition temperature. This indicates that slight rearrangement of FCDs occurs in the Smectic-A phase.

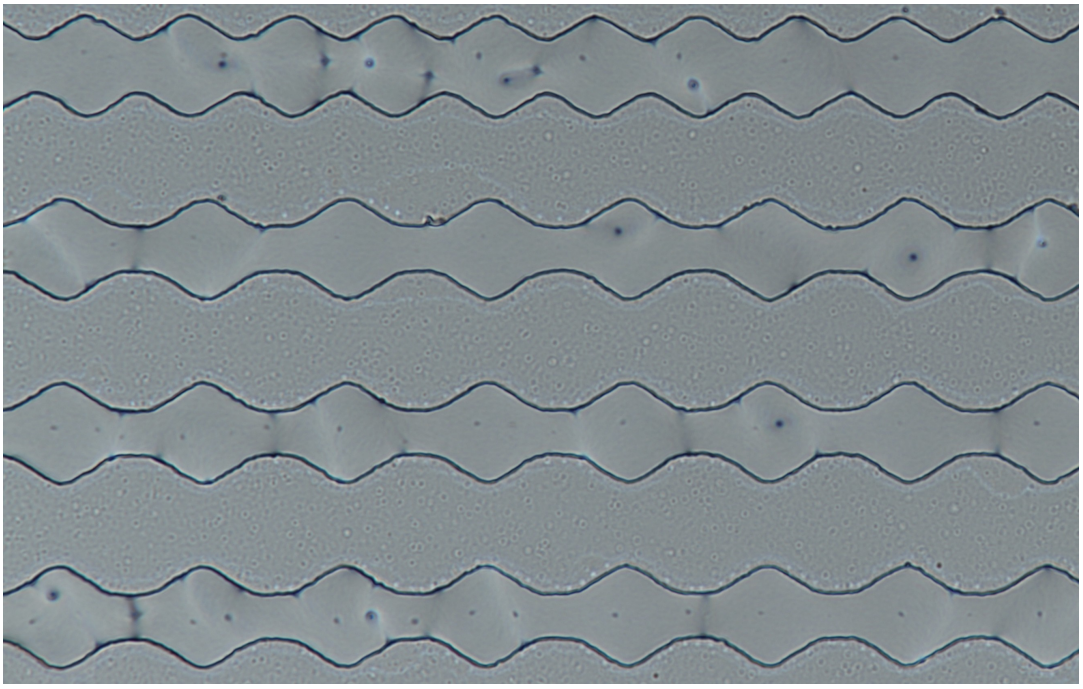

Figure S6: Close-up image of microchannels taken in the nematic phase with brightfield microscopy. Disclinations are visible as black spots. This image was taken at 33.3C, with 33.1C being the smectic-nematic transition (as measured with our specific setup and temperature controller), for reference.

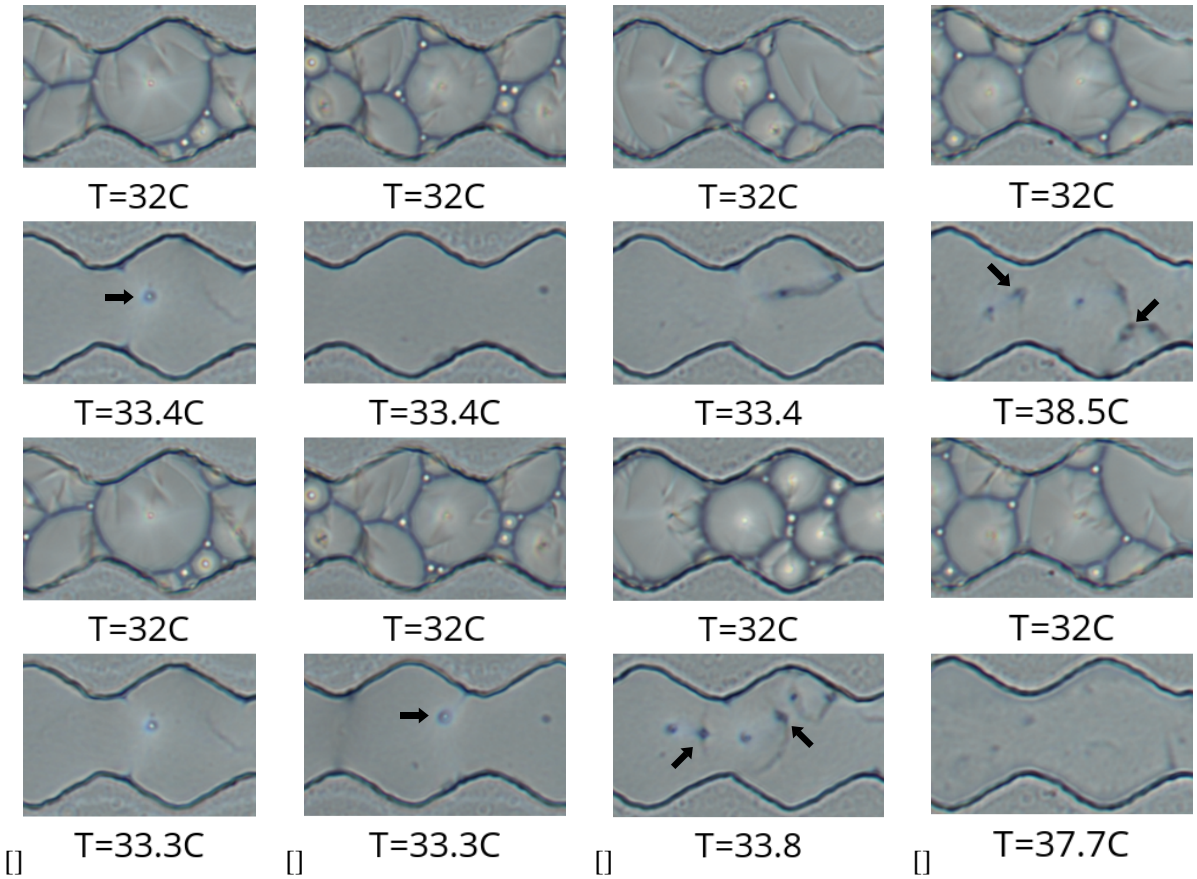

Figure S7: Successive closeups of microchannels to show the evolution of boojums in the nematic phase in between temperature ramps. The columns (a-d) represent different sequences of images taken at different locations. Within each column, four images (arranged vertically) are taken in chronological order during a temperature ramp, with temperatures indicated below each image. In (a-d), the first (uppermost) image is taken in the smectic phase before heating and the third image is taken again in the smectic phase after heating/cooling. The images in the second and fourth rows are taken respectively during the first heating/cooling cycle and during subsequent heating. Black arrows are pointed towards boojums in images taken in the nematic phase. (a) This image sequence shows a +1 diverging boojum that is fixed at its position throughout successive ramps both in smectic and nematic phase. This is an example of a defect pinned by a dust speckle or surface impurity. (b) In this position we see a +1 diverging boojum that seems to be lost in the first heating/cooling cycle (the second image is taken after heating to isotropic phase and cooling in nematic phase) but then reappears at the center of a FCD and is finally visible in the nematic phase after heating to nematic. (c) This sequence shows initially a large FCD and some neighboring small FCDs. In nematic phase after heating to isotropic (second row), only two boojums are visible, one of which with negative topological charge. While cooling again in smectic phase, only small FCDs form, with the boojums in between them. Upon reheating, more boojums become visible. (d) The last column show defects that are still visible while in the nematic phase (possibly +1 converging boojums, observed rarely in our microchannels). The second row is taken before the sample is brought to the isotropic phase. Upon cooling the FCDs are maintained, but upon subsequent heating some of the boojums disappear.